ELSEVIER

Polymer Vol. 37 No. 1, pp. 1–6, 1996

0032-3861/96/$15.00+0.00

polymer papers

Wide-angle X-ray scattering studies using an area detector: crystallite orientation in semicrystalline PET structures

U. Göschel*, K. Deutscher† and V. Abetz‡
Max-Planck-Institute für Polymerforschung, Postfach 3148, 55021 Mainz, Germany
(Received 28 January 1994; revised 19 December 1994)

By means of a Nicolet area detector, the crystallite orientation of uniaxially multi-step drawn poly(ethylene terephthalate) (PET) film strips with large draw ratios from 5.4 to 7.3 has been studied. As orientation parameters, $\langle \cos^n \phi \rangle$, $\langle P_2(\cos\phi) \rangle$ and $\langle P_4(\cos\phi) \rangle$ were determined from the equatorial wide-angle X-ray scattering reflexes (0 1 0), ($\bar{1}$ 1 0) and (1 0 0), where ϕ corresponds to the angle between the drawing direction and the normal of the chosen (hkl) lattice planes. Using both the experimental $\langle \cos^2 \phi_{hk0} \rangle$ and Wilchinsky's method, the crystallite orientation was calculated in terms of the mean-square cosine of the angle σ between the c-axis of the unit cell and the drawing direction. For the highly drawn and semicrystalline structures, the results reveal a nearly perfect alignment of the crystallite c-axis along the drawing direction with a narrow orientation distribution. Despite large variations of the drawing conditions leading to significant differences in the superstructure as well as the Young's modulus, only slight changes of the crystallite orientation are observed.

(Keywords: two-dimensional wide-angle X-ray scattering; crystallite orientation; poly(ethylene terephthalate))

INTRODUCTION

The orientation of molecular chains as a structural feature strongly influences many physical properties, such as the mechanical and optical properties. The definition of orientation can be applied on several structural levels. With regard to wide-angle X-ray scattering (WAXS) studies, orientation of the crystallites is detectable.

Uniaxial drawing procedures can be applied to poly(ethylene terephthalate) (PET) to achieve large draw ratios from 5.4 to 7.3, a birefringence of $0.202 \leq \Delta n \leq 0.249$, and a degree of order of $26 < L_{\bar{1}05}/L \leq 39\%$. Here, $L_{\bar{1}05}$ and L denote the crystal thicknesses obtained from the half-width of the ($\bar{1}$ 0 5) reflection and the meridional long period from small-angle X-ray scattering (SAXS) measurements, respectively. Studies on these structures have revealed that the drawing conditions have a strong influence on the material stiffness (elastic modulus)[1,2], the time- and temperature-dependent deformation behaviour[3] and the lamellar/fibrillar structure[2,4]. The quasi-static elastic modulus at low deformation speed ($d\epsilon/dt \leq 0.5\%\,min^{-1}$) was found[1] to be between 7.1 and 16.8 GPa, compared with 2.0 GPa for isotropic and non-crystalline PET[5]. Recent SAXS investigations on oriented and semicrystalline PET[4] have described a lamellar structure with comparably short lamellae, whereby the lamellae normal can be inclined with respect to the drawing direction. Depending on the drawing conditions, an inclination angle from 0 to 52° is determined.

Since large changes in deformation behaviour and lamellar/fibrillar structure are observed with drawing, information about the crystallite orientation under such conditions could increase our knowledge of the underlying deformation mechanism. Therefore, two-dimensional WAXS investigations have been performed on the same highly drawn PET samples as used in refs 1–4.

THEORETICAL BACKGROUND

Description of orientation

Considering the crystallites as structural units, the orientation development with respect to the sample coordinate system (X_S, Y_S, Z_S) can be described by the angles ϕ_{hkl} and β_{hkl} (refs 6 and 7). According to *Figure 1*, the angles ϕ_{hkl} and β_{hkl} correspond to the angles between Z_S and p_{hkl}, and between X_S and the projection of p_{hkl} in the X_S-Y_S plane, respectively. Z_S denotes the drawing direction and p_{hkl} the normal to the chosen (hkl) lattice planes, specified by the Miller indices. In the following, ϕ and β will be taken for ϕ_{hkl} and β_{hkl}, respectively. The average orientation functions $\langle \cos^n \phi \rangle$ can be calculated from the scattering intensities $I(\phi)$

* To whom correspondence should be addressed. Present address: Tokyo University of Agriculture and Technology, Department of Material Systems Engineering, Koganei, Tokyo 184, Japan
† Present address: Balzers-Pfeiffer GmbH, Emmeliusstraße 33, D-35614 Aßlar, Germany
‡ Present address: Johannes Gutenberg-Universität Mainz, Institut für Organische Chemie, Postfach 3980, D-55099 Mainz, Germany

according to:

$$\langle \cos^n \phi \rangle = \frac{\int_0^{\pi} I(\phi) \cos^n \phi \sin \phi \, d\phi}{\int_0^{\pi} I(\phi) \sin \phi \, d\phi} \quad (1)$$

where

$$I(\phi) = \int_0^{2\pi} I(\phi, \beta) \, d\beta \quad (2)$$

The brackets $\langle\ \rangle$ will be used for average values. In the case of a β-dependence, the scattering intensities $I(\phi, \beta)$ must be first integrated over β according to equation (2) and second over ϕ using equation (1)[6].

The orientation distribution can be written in terms of spherical harmonic functions (Legendre polynomials)[7,8]:

$$\rho(\phi) = \sum_{n=0}^{\infty} (n + \tfrac{1}{2}) \langle P_n(\cos \phi) \rangle P_n(\cos \phi) \quad (3)$$

For symmetry reasons, only polynomials with even order play a role. The second and fourth Legendre polynomials are:

$$\langle P_2(\cos \phi) \rangle = \tfrac{1}{2}(3\langle \cos^2 \phi \rangle - 1) \quad (4)$$

$$\langle P_4(\cos \phi) \rangle = \tfrac{1}{8}(35\langle \cos^4 \phi \rangle - 30\langle \cos^2 \phi \rangle + 3) \quad (5)$$

For a given normal to the $(h\,k\,l)$ plane of the unit cell, the function $\langle \cos^2 \phi \rangle$ assumes values of 1 for a perfect alignment with Z_S as the drawing axis, 1/3 for random orientation, and 0 for precise perpendicularity to Z_S. The corresponding values for $\langle \cos^4 \phi \rangle$ are 1, 1/5 and 0, respectively. According to equations (4) and (5), $\langle P_2(\cos \phi) \rangle$ takes on the respective values 1, 0 and −0.5 and $\langle P_4(\cos \phi) \rangle$ the values 1, 0 and 0.375.

The crystallite orientation of PET in terms of the angle σ between the c-axis of the unit cell and the drawing direction Z_S can be characterized by the normal on the $(\bar{1}\,0\,5)$ lattice plane as well as by using the three equatorial reflexes $(0\,1\,0)$, $(\bar{1}\,1\,0)$ and $(1\,0\,0)$ according to Wilchinsky's method[9,10]. Because of the triclinic unit cell of PET[11], there is no $(0\,0\,1)$ reflex[12]. According to Dumbleton and Bowles[13], the normal of the $(\bar{1}\,0\,5)$ lattice plane reveals the smallest angle to the c-axis of 8–10° for all resolvable reflections of PET. The $(\bar{1}\,0\,5)$ reflex is found to occur at a large scattering angle, $2\theta \approx 43°$, see refs 2, 12 and 13. Using Wilchinsky's method[9,10] to determine the crystallite orientation of PET, the mean-square cosine of σ can be calculated from the experimental $\langle \cos^2 \phi_{hk0} \rangle$ of the three equatorial reflexes (*Figure 2*) and

$$\langle \cos^2 \sigma \rangle = 1 - A\langle \cos^2 \phi_{010} \rangle - B\langle \cos^2 \phi_{\bar{1}10} \rangle - C\langle \cos^2 \phi_{100} \rangle \quad (6)$$

where the parameters $A = 0.8786$, $B = 0.7733$ and $C = 0.3481$ are derived from the triclinic crystal system[9,10]. As seen in *Figure 2*, the $(0\,1\,0)$, $(\bar{1}\,1\,0)$ and $(1\,0\,0)$ lattice planes are parallel to the c-axis.

EXPERIMENTAL

Sample preparation

The WAXS experiments were carried out on uniaxially drawn PET film strips. The drawing conditions are given in *Table 1*. The sample designation coincides with those of our previous studies[1–4]. A nearly isotropic and non-crystalline PET film, with $M_w \approx 20\,000$, thickness of 180 μm and width of 2.8 mm, was used as the precursor material for a multi-step drawing procedure, characterized by the number of temperature steps. The first

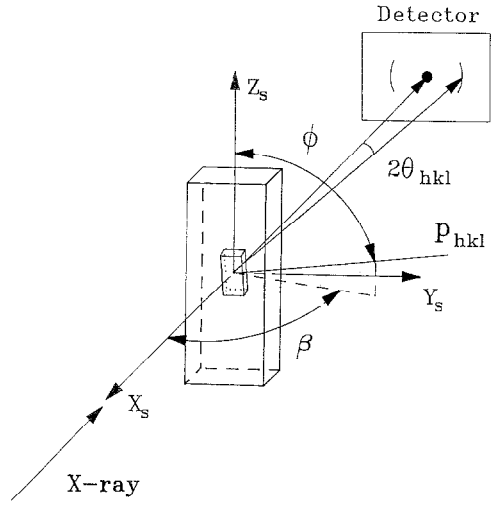

Figure 1 Relationship between the sample coordinate system (X_S, Y_S, Z_S) and the normal to the $(h\,k\,l)$ lattice planes, p_{hkl}

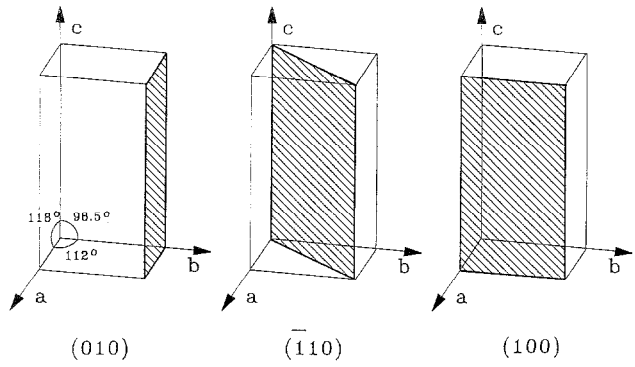

Figure 2 Unit cell planes which correspond to the equatorial scattering reflexes $(0\,1\,0)$, $(\bar{1}\,1\,0)$ and $(1\,0\,0)$. The angle between the normal of the unit cell planes and the drawing direction is denoted as ϕ

Table 1 Zone drawing conditions in the last drawing step. The drawing velocity was 100 mm min^{-1} and the drawing stress was increased step-by-step in 50 MPa increments. The draw ratios are averaged values[1]

			Drawing conditions in the last step		
Sample	Initial sample	Total drawing steps	Drawing temperature, T_d (°C)	Drawing stress range, σ_d (MPa)	Final draw ratio, $\langle\lambda\rangle$
1	isotropic	1	68	15[a]	4.3
2	1	2	160	70–350	6.3
3	2	3	200	200–370	7.1
4	2	3	230	200–400	7.3
5	1	2	200	200–400	7.2
6	isotropic	1	80	38[a]	5.6
7	6	2	160	70–250	6.2
8	isotropic	1	23	[b]	4.2
9	8	2	180	100[a]	5.4

[a] Single-step drawing, drawing velocity of 5.5 mm min^{-1} for sample 1
[b] Single-step drawing in a homogeneous temperature field, drawing velocity of 3 mm min^{-1}

drawing step at 68°C yielded sample 1 and the drawing at 23°C resulted in sample 8 (*Table 1*). Both temperatures are lower than the glass transition temperature (T_g) of 69°C, determined by d.s.c. measurements. Samples 1 and 8 are non-crystalline. Further drawing[2] of these samples at temperatures far above T_g (*Table 1*) caused highly oriented and semicrystalline structures with large average draw ratios up to 7.3. To avoid chain breaks, the drawing stresses in the second and third steps were increased step-by-step in 50 MPa increments[1] until the stress limit was reached. The initial stress in the second drawing step was chosen to be 70 MPa for samples 2 and 7, and 200 MPa for sample 5. Due to the higher temperature, the ultimate drawing stress of the third step was somewhat larger than that of the second step (*Table 1*).

Sample 6 was drawn in only one step at 80°C, which is slightly above the glass transition. The drawing stress of 38 MPa was very large and near the breaking point. Therefore, strain-induced crystallization could occur[2]. The resulting degree of order, $L_{\bar{1}05}/L$, of about 30% was comparable with those of samples drawn in two and three steps[2]. A further drawing of sample 6 at $T = 160$°C yielded sample 7 (*Table 1*).

Wide-angle X-ray scattering

The two-dimensional WAXS studies were performed by means of a Nicolet area detector in conjunction with an 18 kW rotating Cu-anode X-ray source (Rigaku RU-300). A graphite double monochromator, an Ni filter and a set of collimators placed ahead of the sample holder provided a CuKα radiation beam with a wavelength of $\lambda = 0.154$ nm and a point focus diameter of ~1.0 mm. A beam divergence of 0.056° was determined. The WAXS experiments were performed with the horizontal X-ray beam perpendicular to the $Z_S - Y_S$ sample film plane and by changing the angle β in steps of 10°. The distance between sample and detector was chosen as $s = 100$ mm. To obtain a large signal-to-noise ratio, a data recording time of 4 h was used for a sample thickness from 60 to 90 μm. The resolution of the detector was limited by an array of 512 × 512 pixels with a pixel-to-pixel distance of $z = 0.2$ mm. A PCS/CADMUS 9600 computer and a VAX station 3100 including a PV-wave software system (Precision Visuals Inc.) were taken for the instrument control and the interactive data analysis, respectively. The experiment provided the scattering intensities $I(\phi_{hkl})$ for each sample rotation angle β (*Figure 1*). Standard procedures were used for the correction of the detector sensitivity, primary beam profile and amorphous background.

The irradiated volume of the sample varies with the angle β, and part of the incident beam is absorbed by the sample. The absorption was corrected for each sample depending on β. Absorption coefficients, μ, from 9.215 to 9.286×10^{-4} μm^{-1} were found for the PET samples. Variation of the sample thickness has revealed only a negligible influence on $\langle \cos^2 \phi_{hk0} \rangle$ and $\langle \cos^4 \phi_{hk0} \rangle$.

Starting from the two-dimensional WAXS patterns (e.g. *Figure 3*), the intensity distribution $I(\phi_{hk0})$ along the Debye ring (2θ = const.) was determined for each of the three equatorial ($hk0$) reflexes. Usually, reflex intensities from neighbouring Debye rings influence the desired azimuthal intensity distribution $I(\phi_{hk0})$. The tails of these disturbing reflex intensities cause additional

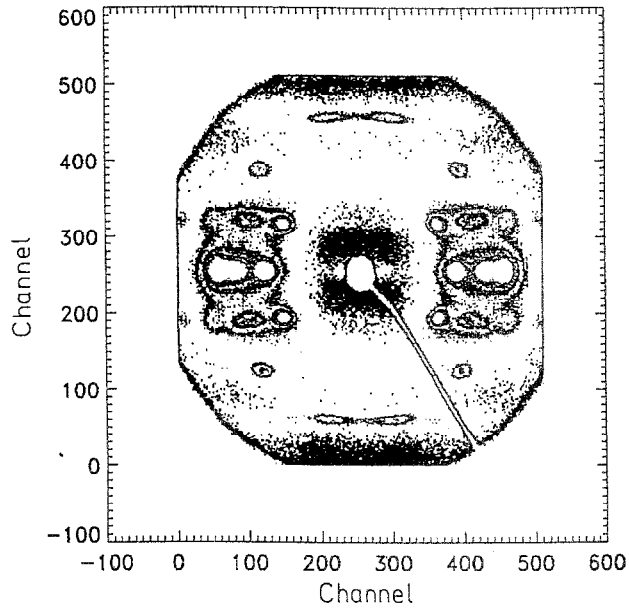

Figure 3 WAXS pattern of the highly oriented and semicrystalline PET sample 3. The X-ray beam is perpendicular to the $Z_S - Y_S$ sample film plane. The drawing direction is vertical

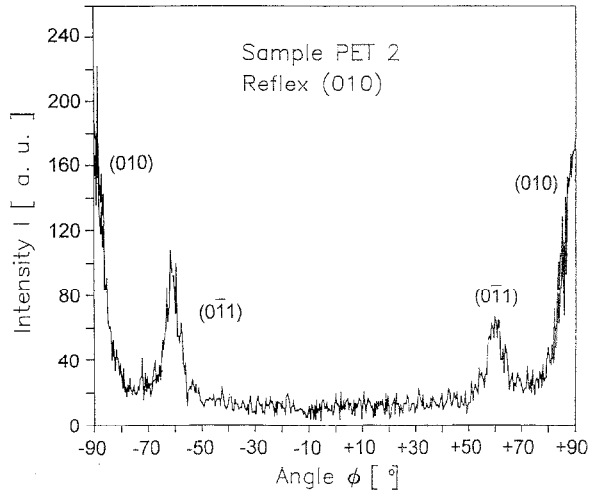

Figure 4 Measured scattering intensity $I(\phi)$ of sample 2 along the Debye ring for the equatorial (0 1 0) reflex. The neighbouring (0 1 1) reflex intensities overlap the desired (0 1 0) reflex. The X-ray beam is perpendicular to the $Z_S - Y_S$ sample film plane

intensity peaks. They are separated by extrapolating the monotonic function $I(\phi_{hk0})$ in the ϕ range from −90 to 90° through the additional peaks (*Figure 4*). The orientation functions $\langle \cos^n \phi_{hk0} \rangle$ were calculated according to equations (1) and (2) from $I(\phi_{hk0})$ along the Debye rings.

RESULTS AND DISCUSSION

Figure 5 presents the two-dimensional scattering pattern of sample 1, which was obtained by cold drawing of the isotropic and non-crystalline precursor film (*Table 1*). The scattering pattern of sample 1 reveals no crystalline reflexes. Contrary to the isotropic initial structure, a broad intensity maximum on the equator exists. The intensity distribution above reflects a highly oriented and non-crystalline structure[14]. In addition to the equatorial

scattering intensity with measured maximum at $2\theta = 21.6°$, a weak reflection close to the meridian at $2\theta = 25.7°$ is found which can be attributed to the conformational regularity. The scattering pattern of sample 1 represented in *Figure 5* corresponds to that of sample 8. Both structures characterize the initial materials for all the semicrystalline structures discussed in the present paper.

Figure 6 reveals the known eight intensive reflexes for the semicrystalline PET samples 2–5, 7 and 9 in the angular range $2\theta = 3$ to 30°, corresponding to the Miller indices $(h\,k\,l)$ with $l = 0$ to 3. The angles 2θ are calculated from the two-dimensional scattering patterns according to

$$2\theta = \arctan\left(\frac{rz}{s}\right) \qquad (7)$$

with the Debye ring radius r (number of channels), pixel distance z and sample-to-detector distance s. The reflex designation is taken from Bonart[15] and Jungnickel[16]. The angular positions correspond to those in the scattering patterns of samples 2–5, 7 and 9. Almost independent of the drawing conditions, the three equatorial reflexes at (0 1 0), ($\bar{1}$ 1 0) and (1 0 0) are found at scattering angles $2\theta = 17.3$, 22.5 and 25.7°, respectively. As known, the peak position is determined by the geometry and size of the unit cell. Within the accuracy of the WAXS experiment applied, no significant variation of the crystal plane spacings with drawing is found for samples 2–5, 7 and 9. Fakirov *et al.*[17] have also reported negligible differences in spacings for PET samples annealed at different temperatures between 120 and 260°C. In contrast, the strain-induced crystallized sample 6 reveals a unit cell dimension different from those of the other semicrystalline samples. Preparing sample 7 from sample 6 (*Table 1*) shows that the crystal plane spacings can be influenced by drawing and heat setting as discussed by Bhatt *et al.*[18] as well as by Gupta and Kumar[19].

Tables 2–4 present the orientation parameters of semicrystalline PET calculated by means of equations (1), (2), (4) and (5). The equatorial reflexes (0 1 0), ($\bar{1}$ 1 0) and (1 0 0) correspond to the lattice planes parallel to the molecular c-axis of the unit cell, schematically represented in *Figure 2*. According to Daubeny *et al.*[11], the unit cell is triclinic with angles of $(c, a) = 98.5°$, $(c, b) = 118°$ and $(a, b) = 112°$. The angles ϕ_{hkl} between the drawing direction Z_S and the normal of the $(h\,k\,l)$ lattice planes above are expressed in terms of the orientation parameters given in *Tables 2–4*. The data reveal that the normals of the chosen three lattice planes are almost perpendicular to the drawing direction. Only slight angular variations with the drawing conditions are found. In the case of the (1 0 0) reflex, the differences in the orientation parameters among the PET samples are somewhat larger than for the ($\bar{1}$ 1 0) and (0 1 0) reflexes.

The uniaxially drawn PET samples have been investigated for biaxial orientation components. For all sample rotation angles β, three sharp equatorial reflexes are found. The proportion of the maximum intensities among the equatorial reflexes can vary with β (*Figure 7*). In the case of sample 5, the scattering intensities $I(\phi_{hk0})$ are found to be independent of β. To illustrate these results, the intensity distributions along the equatorial

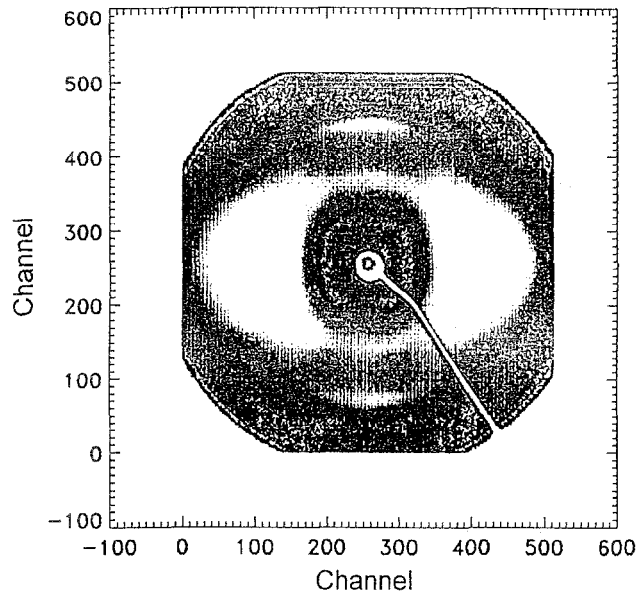

Figure 5 WAXS pattern of the oriented and non-crystalline PET sample 1, where the X-ray beam is perpendicular to the $Z_S - Y_S$ sample film plane. The drawing direction is vertical

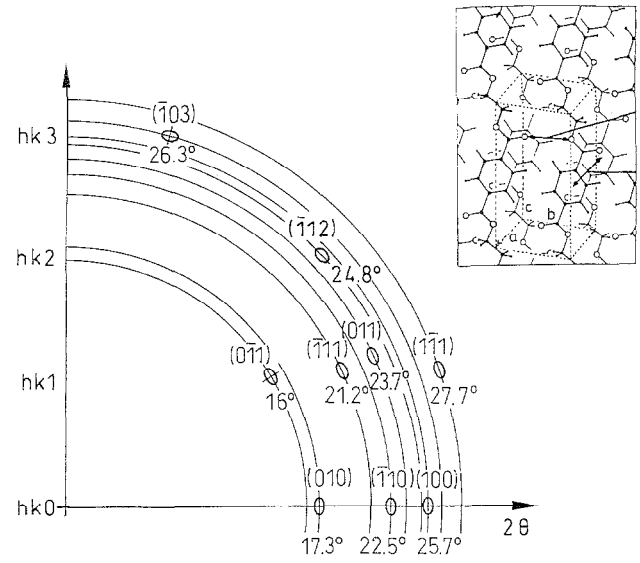

Figure 6 Schematic representation of WAXS reflexes for oriented and semicrystalline PET. The reflex designation is taken from refs 14 and 15. The angular position corresponds to those of samples 2–5, 7 and 9

Table 2 Orientation parameters from the (0 1 0) reflex

Sample	Orientation parameters $\langle\cos^2\phi\rangle$ ±0.0005	$\langle P_2(\cos\phi)\rangle$ ±0.0008
2	0.0023	−0.4964
3	0.0016	−0.4976
4	0.0015	−0.4978
5	0.0020	−0.4970
6	0.0079	−0.4882
7	0.0036	−0.4946
9	0.0021	−0.4969

(0 1 0), ($\bar{1}$ 1 0) and (1 0 0) reflexes of samples 3 and 5 using the X-ray beam perpendicular to the $Z_S - Y_S$ as well as to the $Z_S - X_S$ sample film planes are presented in *Figure 7*. Despite differences in the scattering intensities $I(\phi_{hk0})$ with β, the studies reveal a relative change of $\langle P_2(\cos\phi)\rangle$

which is smaller than 0.8%. Therefore, the β-dependence can be neglected for the PET samples above.

The crystallite orientation is calculated in terms of $\langle\cos^2\sigma\rangle$ according to equation (6), where σ is the angle between the c-axis of the unit cell and the drawing direction, Z_S. As seen in *Table 5*, the crystallites are well oriented. The angles σ as averaged values from the orientation distribution according to $\langle\cos^2\sigma\rangle$ are found in the range from 2.9 to 7.7° for the highly drawn and semicrystalline PET samples 2–9. Such small values are only possible in the case of a very narrow orientation distribution. This is in good agreement with the orientation parameters $\langle P_2(\cos\phi)\rangle$ presented in *Tables 2–4*. The $\langle\cos^4\phi\rangle$ are within the error estimates and, therefore, not listed together with the resulting $\langle P_2(\cos\phi)\rangle$. Both $\langle P_2(\cos\phi)\rangle$ and $\langle P_4(\cos\phi)\rangle$ are close to the limits for perfect perpendicular orientation of the hkl plane normals to the drawing direction.

The lowest crystallite orientation among the semicrystalline samples is found for the strain-induced crystallized sample 6. Here, the crystallization took place at 80°C, near the glass transition. The achievable drawing stress was only low with 38 MPa (*Table 1*). Further drawing of that sample caused a significant improvement of the crystallite orientation. However, the final orientation reached was lower than those for samples 2–5 which were crystallized under hot drawing conditions.

As seen from the comparison of the highly drawn sample 2 with sample 3 or 4, an additional drawing step can yield a small improvement in the crystallite orientation. Such a change in the orientation was connected with a large increase in the draw ratio from 6.3 to 7.1 or 7.3, respectively (*Table 1*).

Remarkably, the two-step drawn sample 5, which was loaded at a very large initial stress in the second step, reveals almost the same perfect crystallite orientation as samples 3 and 4 which experienced an additional drawing temperature at 160°C and much more incremental drawing stress increases in the second drawing

Table 3 Orientation parameters from the $(\bar{1}\,1\,0)$ reflex

Sample	Orientation parameters	
	$\langle\cos^2\phi\rangle$ ±0.0005	$\langle P_2(\cos\phi)\rangle$ ±0.0008
2	0.0055	−0.4918
3	0.0050	−0.4925
4	0.0013	−0.4981
5	0.0019	−0.4972
6	0.0074	−0.4889
7	0.0045	−0.4933
9	0.0024	−0.4964

Table 4 Orientation parameters from the (1 0 0) reflex

Sample	Orientation parameters	
	$\langle\cos^2\phi\rangle$ ±0.0005	$\langle P_2(\cos\phi)\rangle$ ±0.0008
2	0.0054	−0.4919
3	0.0013	−0.4981
4	0.0008	−0.4988
5	0.0009	−0.4987
6	0.0158	−0.4763
7	0.0022	−0.4967
9	0.0017	−0.4975

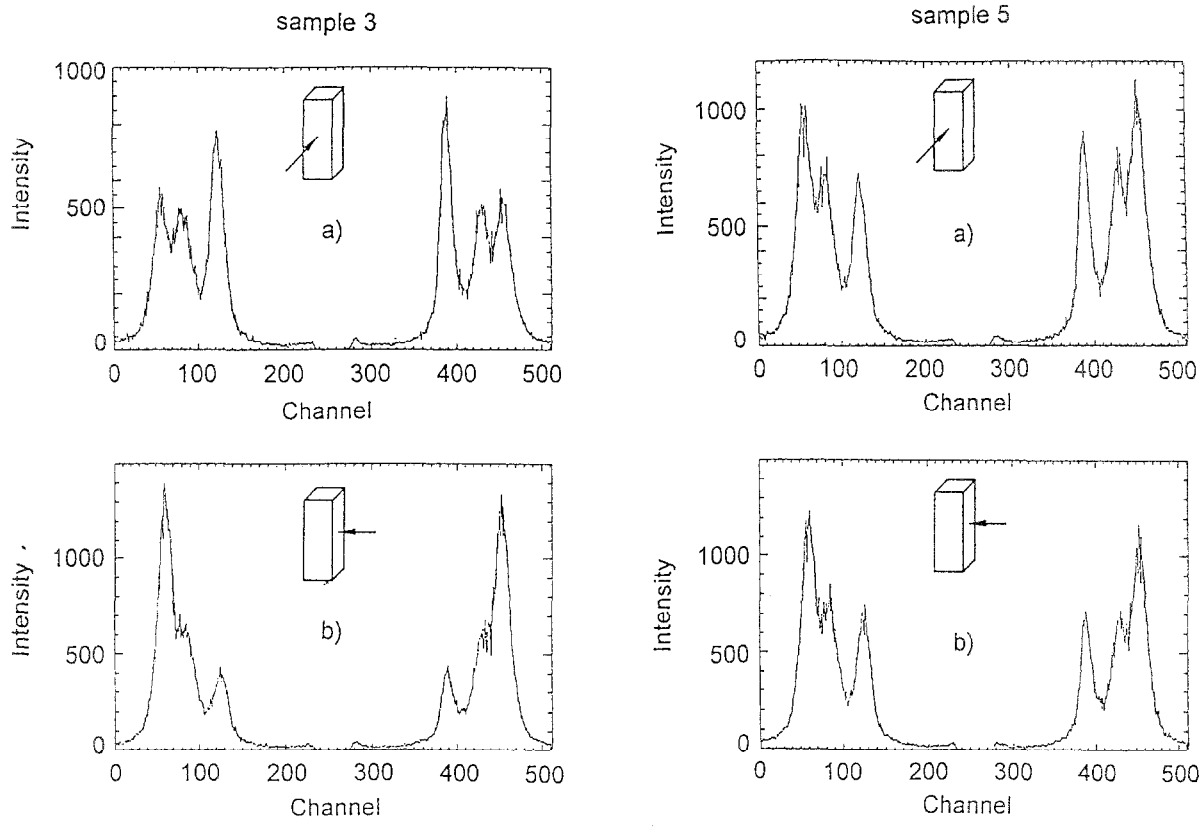

Figure 7 Measured scattering intensity $I(\phi)$ of samples 3 and 5 along the equator. Represented are the three $(hk0)$ reflexes, (0 1 0), $(\bar{1}\,1\,0)$ and (1 0 0), along the equator. The X-ray beam is perpendicular to the Z_S-Y_S plane (a) and the Z_S-X_S sample film plane (b)

Table 5 Crystallite orientation

Sample	Orientation parameters	
	$\langle\cos^2\sigma\rangle$	$\langle\sigma\rangle$ (°)
2	0.9917 ± 0.0010	5.2 ± 0.4
3	0.9942 ± 0.0010	4.4 ± 0.4
4	0.9974 ± 0.0011	2.9 ± 0.6
5	0.9964 ± 0.0011	3.4 ± 0.5
6	0.9819 ± 0.0010	7.7 ± 0.2
7	0.9925 ± 0.0010	5.0 ± 0.4
9	0.9957 ± 0.0010	3.8 ± 0.5

step. The final drawing stresses reached at draw ratios from 7.1 to 7.3 (*Table 1*) are comparable and lie in the range between 370 and 400 MPa.

CONCLUSIONS

PET films were multi-step drawn close to the draw ratio limit at each temperature. Previous studies on these highly drawn materials revealed large differences in the superstructure as well as the mechanical properties with variation of the drawing conditions. The present WAXS investigations concerning the crystallite orientation of these semicrystalline PET samples reveal a nearly perfect alignment of the *c*-axis with respect to the drawing direction, expressed by an averaged angle σ from 2.9 to 7.7°. According to the orientation parameters $\langle P_2(\cos\phi)\rangle$ and $\langle P_4(\cos\phi)\rangle$ for the normals of the (0 1 0), (1 1 0) and (1 0 0) lattice planes, the orientation distribution is very narrow. Additional drawing steps may improve the crystallite orientation. Suddenly applied very large drawing stresses on an oriented and non-crystalline structure can also yield a perfect crystallite orientation, comparable to those reached by additional drawing treatments. Hot drawing of an oriented and non-crystalline PET structure yields a higher final crystallite orientation than achievable by strain-induced crystallization close to the glass transition.

REFERENCES

1 Göschel, U. *Acta Polymerica* 1989, **40**, 23
2 Hofmann, D., Göschel, U., Walenta, E., Geiß, D. and Philipp, B. *Polymer* 1989, **30**, 242
3 Göschel, U. *Polymer* 1992, **33**, 1881
4 Göschel, U. *Polymer* submitted
5 Göschel, U. and Nitzsche, K. *Acta Polymerica* 1985, **36**, 580
6 Alexander, L. E. 'X-ray Diffraction Methods in Polymer Science', Wiley-Interscience, New York, 1969
7 Stein, R. S. and Wilkes, G. L. in Ward, I. M. 'Structure and Properties of Oriented Polymers', Applied Science Publishers, London, 1975
8 Windle, A. H. in Ward, I. M. 'Developments in Oriented Polymers—1', Applied Science Publishers, London, 1982
9 Wilchinsky, Z. W. *J. Appl. Phys.* 1959, **30**, 792
10 Wilchinsky, Z. W. 'Advances in X-ray Analysis', Plenum Press, New York, 1963, Vol. 6
11 Daubeny, R. de P., Bunn, C. W. and Brown, C. J. *Proc. R. Soc. (London)* 1954, **A226**, 531
12 Ledbetter, M., Cuculo, J. and Tucker, P. *J. Polym. Sci., Polym. Chem. Edn* 1984, **22**, 1435
13 Dumbleton, J. H. and Bowles, B. B. *J. Polym. Sci., A-2* 1966, **4**, 951
14 Pakula, T. and Fischer, E. W. *J. Polym. Sci., Phys. Edn* 1981, **19**, 1705
15 Bonart, R. *Kolloid Z.-Z. Polym.* 1966, **213**, 1
16 Jungnickel, B.-J. *Angew. Makromol. Chem.* 1984, **125**, 121
17 Fakirov, S., Fischer, E. W. and Schmidt, G. F. *Makromol. Chem.* 1975, **176**, 2459
18 Bhatt, G. M., Bell, J. P. and Knox, J. R. *J. Polym. Sci. A-2*, 1976, **14**, 373
19 Gupta, V. B. and Kumar, S. *J. Polym. Sci.* 1981, **26**, 1865